

Industrially fabricated single-electron quantum dots in Si/Si-Ge heterostructures*

Till Huckemann,^{1,†} Pascal Muster,^{2,‡} Wolfram Langheinrich,² Varvara Brackmann,³ Michael Friedrich,³ Nikola D. Komerički,⁴ Laura K. Diebel,⁵ Verena Stieß,⁵ Dominique Bougeard,⁵ Yuji Yamamoto,⁶ Felix Reichmann,⁶ Marvin H. Zöllner,⁶ Claus Dahl,² Lars R. Schreiber,^{1,7} and Hendrik Bluhm^{1,7}

¹*JARA Institute for Quantum Information, RWTH Aachen University, 52062 Aachen, Germany*

²*Infineon Technologies Dresden GmbH & Co. KG, Königsbrücker-Str. 180, 01099 Dresden*

³*Fraunhofer Institute for Photonic Microsystems,*

Center for Nanoelectronic Technologies, An der Bartlke 5, 01099 Dresden, Germany

⁴*Fraunhofer Institute for Applied Solid State Physics IAF, Tullastr. 72, 79108 Freiburg, Germany*

⁵*Fakultät für Physik, Universität Regensburg, 93040 Regensburg, Germany*

⁶*IHP – Leibniz-Institut für innovative Mikroelektronik, 15236 Frankfurt (Oder), Germany*

⁷*ARQUE Systems GmbH, 52074 Aachen, Germany*

(Dated: 17.02.2025)

This paper reports the compatibility of heterostructure-based spin qubit devices with industrial CMOS technology. It features Si/Si-Ge quantum dot devices fabricated using Infineon's 200 mm production line within a restricted thermal budget. The devices exhibit state-of-the-art charge sensing, charge noise and valley splitting characteristics, showing that industrial fabrication is not harming the heterostructure quality. These measured parameters are all correlated to spin qubit coherence and qubit gate fidelity. We describe the single electron device layout, design and its fabrication process using electron beam lithography. The incorporated standard 90 nm back-end of line flow for gate-layer independent contacting and wiring can be scaled up to multiple wiring layers for scalable quantum computing architectures. In addition, we present millikelvin characterization results. Our work exemplifies the potential of industrial fabrication methods to harness the inherent CMOS-compatibility of the Si/Si-Ge material system, despite being restricted to a reduced thermal budget. It paves the way for advanced quantum processor architectures with high yield and device quality.

Keywords: Quantum computing, Quantum well devices, Single electron devices, Fabrication

I. INTRODUCTION

Universal quantum computers with error correction will require orders of magnitude more qubits than available today. Semiconductor qubits offer the perspective to take advantage of very large scale integration (VLSI) technology that can easily achieve such a complexity for classical electronics. Using devices fabricated in academic labs, all required qubit operations [1–3], few-qubit devices [4, 5] and qubit shuttling as a scalability element [6–8] have been demonstrated. Now, the transfer to industrial fabrication techniques is required to achieve a sufficient yield for proposed quantum processor architectures [9–11]. The platforms on which industrial progress has recently been made include fully depleted silicon on insulator (FD-SOI) nanowires [12], FinFET devices [13] and Si/Si-Ge heterostructures [14] using CMOS pilot lines. While the first two types are compatible with planar CMOS processing techniques, heterostructures impose a restricted thermal budget to avoid excessive inter-diffusion at the interfaces [15]. It limits the options for oxide formation to temperatures below $\approx 750^\circ\text{C}$ which raises concerns

regarding oxide quality and thus charge noise. On the other hand, a heterostructure-based quantum well has the advantage of an all-crystalline environment and therefore lower disorder, provided that the dislocation density in the crystalline material is sufficiently low. As a result, multi-quantum-dot and multi-qubit devices have already been realized [4, 5].

Besides yield and qubit quality, as recently demonstrated in Si/Si-Ge [4, 16] using a high- κ gate stack process, the proposed quantum processor architectures also require a Back-End of Line (BEoL) processes for multi-layer wiring schemes.

We report the realization of quantum dot (QD) devices in Si/Si-Ge heterostructures in a 200 mm CMOS production line including a BEoL. Charge sensing and charge noise measurements at $\approx 20\text{ mK}$ reveal state-of-the-art characteristics.

II. DEVICE

As substrate a Si/Si-Ge heterostructure with a 10 nm thin, tensile-strained Si layer (Fig. 1(a)) is used, in which QDs can be electrostatically formed by tuning gate voltages. The devices' symmetric gate layout (Fig. 1) is designed to benchmark charge noise [1, 17] and valley-splitting [18, 19] of QDs, both important performance metrics for the heterostructure quality. Of the two interchangeable QDs formed, one can be used as a charge

* This work has been submitted to the IEEE for possible publication. Copyright may be transferred without notice, after which this version may no longer be accessible.

[†] till.huckemann@rwth-aachen.de

[‡] pascal.muster@infineon.com

sensing dot to determine the electron occupation of the other. The QDs are confined laterally by electrostatic potentials from the gate electrodes in the layer **G1**, as shown in Fig. 1(c). The QD is formed by an accumulating plunger gate (**PI**), two barrier gates (**B1**, **B2**) controlling the coupling to leads, and a gate separating both QDs (**SG**) from each other. A second gate layer **G2** acts as top-gate (**TG**) to globally tune the 2DEG accumulation. The pinch-off gates in G1 are intended to prevent parasitic current paths. The gates are contacted by tungsten vias (**CA**) from the separately defined wiring layer **M1** on top of the interlayer dielectric (**ILD**). The implanted areas (**IM**) of $\approx 2.5 \times 10^3 \mu\text{m}^2$ used as ohmic contacts are defined $\approx 60 \mu\text{m}$ away from the active QD region. The wiring layer is used to accumulate charge carriers between the contacts and the active region, inducing reservoirs in the immediate vicinity of the dots to ensure a small stray capacitance.

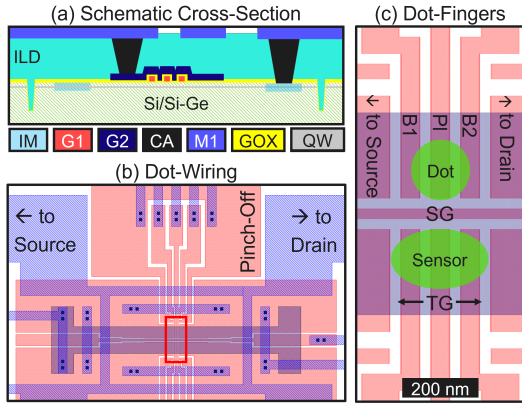


Figure 1. Schematic device cross-section (a) together with the device design labeled with functional names (b) and a zoomed in version for the dot region (c). The implant regions are labeled as **IM**, the two different TiN gate layers as **G1** resp. **G2**, the gate oxides underneath as **GOX**. The dots are contacted via leads induced by the wiring layer **M1**, which is also used for wiring and contacting the gates by tungsten vias labeled as **CA**. The nominal distance between the two QDs is about 100 nm.

Fig. 2 shows a transmission electron microscopy (TEM) of an exemplary QD device comparable to the measured ones and a schematic overview of the process flow.

The Si/Si-Ge heterostructure was epitaxially grown using CVD with natural isotopic composition on 200 mm $\langle 100 \rangle$ Si wafers and was purchased from Lawrence Semiconductor Research Laboratory Inc. The barrier underneath the Si quantum well consists of a several μm thick linearly graded $\text{Si}_{1-x}\text{Ge}_x$ buffer, used for relaxing the Si-Ge, and a several hundred nm thick $\text{Si}_{0.7}\text{Ge}_{0.3}$ barrier on top. The strained Si quantum well of 10 nm thickness is covered by a 30 nm thick $\text{Si}_{0.7}\text{Ge}_{0.3}$ spacer layer. It is terminated with a Si cap layer, thinned to roughly 2 nm by the subsequent gate stack processing. These parameters are similar to those commonly used [16, 18, 20].

The 10 nm thick SiO_2 oxide underneath both G1 and

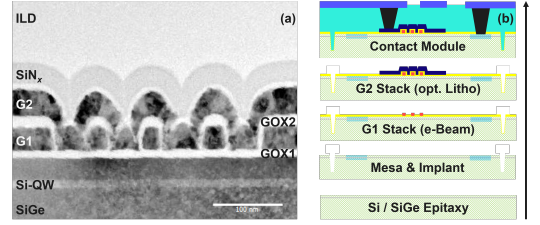


Figure 2. (a) TEM cross-section of an exemplary device & (b) schematic overview of the relevant process steps, colored as in Fig. 1. The TiN metal gates are labeled by their defining layers **G1** and **G2**, the underlying PECVD gate oxides as **GOX1** and **GOX2** respectively. The etch-stop nitride (**SiN_x**) and interlayer dielectric (**ILD**) layers lying on top are necessary for the contact module.

G2 is deposited through low temperature ($\approx 400^\circ\text{C}$) plasma enhanced CVD. This SiO_2 acts as a good dielectric insulator with low leakage and trap density, down to $3 \times 10^{10}/(\text{cm}^2 \text{eV})$. It thus offers an attractive alternative to aluminum oxides – with measured interface trap densities in the range of $3 \times 10^{11}/(\text{cm}^2 \text{eV})$ to $1 \times 10^{12}/(\text{cm}^2 \text{eV})$ (not shown) – or other high- κ dielectrics deposited by Atomic Layer Deposition, which are generally considered to have a lower interface quality [21]. The oxide layers are covered with a 30 nm thick sputtered TiN layer acting as the gate metal for G1 and G2. Only the first fine-patterned gate layer G1 is exposed by an industrially compatible, high-throughput electron-beam lithography (EBL) tool. This is the most effective approach for prototyping and low-volume production [22] on 200 mm without compromising device quality. The second self-aligned gate layer G2 is patterned by optical lithography. The transfer of the photo-resist pattern into the TiN layer after exposure is carried out by dry-etch processes followed by a wet gate stack clean, which removes all metal free gate oxides for subsequent processes. This ensures high-quality oxides without any memory of previous processes introducing defects, charges, or contamination. Subsequently, we process the contact module to contact the double gate stack using a standard 90 nm BEoL.

III. MILLIKELVIN CHARACTERIZATION

We tested more than 10 devices at cryogenic temperatures and provide a detailed report on the characteristics of the first fully functional device, which we measured in a dilution refrigerator with a base temperature of 20 mK. Several other devices gave a similar picture regarding disorder and drift of the quantum dots. By applying wafer-scale cryo-characterization of similar QD devices fabricated in the same way, a leakage ($R > 100 \text{ M}\Omega$), accumulation ($S > 1 \mu\text{S}$) and gate functionality yield $\geq 90\%$ have been achieved.

We start the characterization by finding a set of gate

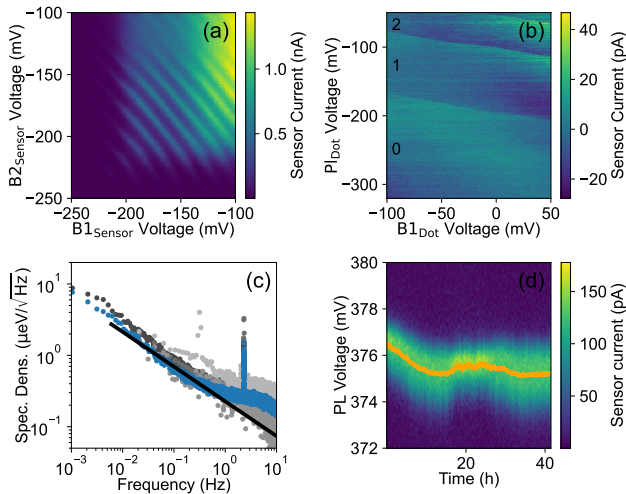


Figure 3. (a) Barrier-Barrier scan of SET with pristine Coulomb oscillations. (b) Charge stability diagram of dot on side 1 measured with side 2 of the device operated as SET. Black numbers indicate the dot occupancy. The sensor background is subtracted to enhance visibility. In (a) and (b), a source-drain bias of 0.1 mV was applied by a lock-in amplifier. (c) Noise spectral density, extracted by Welch’s method from time traces of the sensor current at the flank of a Coulomb oscillation. The Source-Drain-Bias was increased to 300 μ V for these time traces. The black line is a representative fit with $\alpha = -0.97$ to the blue curve. Grey data points correspond to equivalent measurements at different Coulomb peaks. (d) Tracking of a Coulomb peak over ≈ 40 h by continuous PL voltage sweeps. The peak position, extracted by fitting a Gaussian function to the individual traces, is indicated in orange.

voltages that allows the formation of a single-electron transistor (SET) for charge sensing and an adjacent few electron quantum dot, a process called tuning. To this end, we increase the voltages of accumulation gates in G1 and M1, of the topgate TG and the finger gates B1, P1 and B2 to accumulate charge carriers in the quantum well, thus forming a conductive channel. Once a sensor current is observable, we reduce the barrier gates’ voltages to raise tunneling barriers and form a dot close to P1. Using small adjustments to P1, TG and SG, we then form a SET featuring clean Coulomb oscillations as visible in Fig. 3(a). The straightness of the Coulomb lines and absence of resonance features attest low disorder. The symmetry of the device allows us to tune its second dot in analogy to the first one. Note that tuning of the second dot usually requires a re-adjustment of the SET gate’s voltage due to the cross-coupling of the dot and the SET gates. Subsequently, B2 of the dot is closed, which facilitates reaching the few electron regime. Ramping B1’s and P1’s voltages to control tunnel barrier and dot potential, respectively, we measure the charge stability diagram (Fig. 3(b)). Steps reflecting changes of the dot occupancy are clearly visible, and the electron filling can be controlled down to the last electron. Functional

devices show good tunability and can be brought into the single-electron regime within a few hours. Furthermore, variations between multiple thermal cycles for the same device are minor.

As dephasing due to nuclear spins can be reduced significantly by using a Si²⁸ enriched quantum well, charge noise is the most relevant technological parameter determining qubit coherence [1, 17, 23]. It is predominantly influenced by the quality of the gate stack, such as defects in the gate oxide and the oxide-substrate interface [24]. To benchmark long term stability and noise characteristics of the device, we record several time traces of the SET at operation points on the flanks of multiple Coulomb oscillations. We determine the spectral density $\sqrt{S} = \frac{\alpha}{dI/dV} \times \sqrt{S_i}$ of the electrochemical potential of the quantum dot with dI/dV the slope of the respective Coulomb peak at the operation point, an averaged lever arm α of 0.076(11) eV/V extracted from Coulomb diamonds and the power spectral density S_i of the current measurement as calculated from the time traces using Welch’s method. The results are shown in Fig. 3(c). The measured lever arm lies within the range of similarly investigated values on related Si/SiGe heterostructures from other groups [16, 20, 25]. Below 0.1 Hz we observe a $f^{\alpha/2}$ behavior with an average of $\alpha = -0.99(4)$. The kink at frequencies around 0.1 Hz is likely caused by the setup’s noise background. Extrapolation of the $f^{\alpha/2}$ behavior at lower frequencies to 1 Hz yields an average noise spectral density of 0.27(5) μ eV/Hz^{0.5}, which is among the lowest values found in devices from academic fabrication [17, 18, 20, 25]. It is comparable to the value resulting from an extensive gate stack optimization reported on Si/Si-Ge [20] with an average of 0.29(2) μ eV/Hz^{0.5}. We obtained similar results in a second cooldown of the same device in a different setup. Coulomb peaks tracked over the course of 40 h exhibit a very low drift with shifts of less than 2 mV. This is an important test, as electron tunneling to states at the Si-SiO₂ interface can lead to strong drift and instability phenomena in some heterostructure-based quantum devices [26, 27].

Another important characteristic of Si/Si-Ge QDs is the energy splitting E_{VS} between the lowest conduction band valleys. It depends on local atomistic details of the Si-Ge heterostructure and small E_{VS} compromise spin qubit operations [28]. Narrower QWs with slightly higher Ge-content or just Ge-inter-diffusion at the QW interfaces increase E_{VS} on average [15, 20]. From magneto-spectroscopy [18] of the consecutive charging lines for a QD occupation from 0 to 3 electrons [29], we deduce $E_{VS} = 50$ μ eV for a dot configuration corresponding to a gate-controlled confinement. This comparatively low value is within the range of values found in a valley splitting mapping for a device fabricated from the same batch of heterostructures by an academic liftoff process [19].

IV. CONCLUSION

We have demonstrated few electron QD devices in Si/Si-Ge heterostructures fabricated within an industrial production line including a high-quality, low-temperature grown PECVD SiO₂, a BEoL process and CMOS-compatible electron-beam lithography. We evaluated the device performance in terms of the quality of Coulomb oscillations of a single-electron transistor, charge noise, single electron detection and valley-splitting. Although the study focuses on few exemplary devices and is to be verified by larger statistics, our findings reveal that the industrial etching process and the limited thermal fabrication budget does not compromise the device performance. On the contrary, the charge-noise and electrostatic disorder in the Si quantum well is remarkably low and a correlation to the low trap density of the gate oxides could be speculated.

We expect that our process is easily adaptable to the realization of Ge quantum dots, which are advantageous regarding all-electrical spin control and lithography requirements but are much more sensitive to charge noise [30]. On either platform, the expected high level of yield and reliability, in contrast to an academic metal lift-off process, and a multilayer BEoL are a prerequisite for two-dimensional quantum processor architectures such as the one proposed by Künne *et al.* [11].

ACKNOWLEDGEMENTS

This work was partially funded by the German Federal Ministry of Education and Research, reference numbers 13N15652, 13N14778, 13N15658, Project QUASAR and Project SiQuBus; the German Research Foundation within the project 289786932 (BO 3140/4-2) and the European Union's Horizon research and innovation program, grant agreement No. 951852, Project QLSI.

-
- [1] J. Yoneda, K. Takeda, T. Otsuka, T. Nakajima, M. R. Delbecq, G. Allison, T. Honda, T. Kodera, S. Oda, Y. Hoshi, N. Usami, K. M. Itoh, and S. Tarucha, *Nature Nanotech* **13**, 102 (2017).
 - [2] A. Noiri, K. Takeda, T. Nakajima, T. Kobayashi, A. Sammak, G. Scappucci, and S. Tarucha, *Nature* **601**, 338 (2022).
 - [3] A. R. Mills, C. R. Guinn, M. J. Gullans, A. J. Sigillito, M. M. Feldman, E. Nielsen, and J. R. Petta, *Sci. Adv.* **8**, eabn5130 (2022).
 - [4] S. G. J. Philips, M. T. Mądzik, S. V. Amitonov, S. L. de Snoo, M. Russ, N. Kalhor, C. Volk, W. I. L. Lawrie, D. Brousse, L. Tryputen, B. P. Wuetz, A. Sammak, M. Veldhorst, G. Scappucci, and L. M. K. Vandersypen, *Nature* **609**, 919 (2022).
 - [5] W. Ha, S. D. Ha, M. D. Choi, Y. Tang, A. E. Schmitz, M. P. Levendorf, K. Lee, J. M. Chappell, T. S. Adams, D. R. Hulbert, E. Acuna, R. S. Noah, J. W. Matten, M. P. Jura, J. A. Wright, M. T. Rakher, and M. G. Borselli, *Nano Lett.* **22**, 1443 (2021).
 - [6] T. Struck, M. Volmer, L. Visser, T. Offermann, R. Xue, J.-S. Tu, S. Trelenkamp, Ł. Cywiński, H. Bluhm, and L. R. Schreiber, *Nat Commun* **15**, 1325 (2024).
 - [7] R. Xue, M. Beer, I. Seidler, S. Humpohl, J.-S. Tu, S. Trelenkamp, T. Struck, H. Bluhm, and L. R. Schreiber, *Nat Commun* **15**, 2296 (2024).
 - [8] M. De Smet, Y. Matsumoto, A.-M. J. Zwerver, L. Tryputen, S. L. de Snoo, S. V. Amitonov, A. Sammak, N. Samkharadze, Ö. Gül, R. N. M. Wasserman, M. Rimbach-Russ, G. Scappucci, and L. M. K. Vandersypen, *High-fidelity single-spin shuttling in silicon* (2024).
 - [9] M. Veldhorst, H. G. J. Eenink, C. H. Yang, and A. S. Dzurak, *Nat Commun* **8**, 1766 (2017).
 - [10] J. M. Boter, J. P. Dehollain, J. P. van Dijk, Y. Xu, T. Hensgens, R. Versluis, H. W. Naus, J. S. Clarke, M. Veldhorst, F. Sebastiano, and L. M. Vandersypen, *Phys. Rev. Applied* **18**, 24053 (2022).
 - [11] M. Künne, A. Willmes, M. Oberländer, C. Gorjaew, J. D. Teske, H. Bhardwaj, M. Beer, E. Kammerloher, R. Otten, I. Seidler, R. Xue, L. R. Schreiber, and H. Bluhm, *Nat Commun* **15**, 4977 (2024).
 - [12] T. Bedecarrats, B. C. Paz, B. M. Diaz, H. Niebojewski, B. Bertrand, N. Rambal, C. Comboroure, A. Sarrazin, F. Boulard, E. Guyez, J.-M. Hartmann, Y. Morand, A. Magalhaes-Lucas, E. Nowak, E. Catapano, M. Casse, M. Urdampilleta, Y.-M. Niquet, F. Gaillard, S. De Franceschi, T. Meunier, and M. Vinet, in *2021 IEEE International Electron Devices Meeting (IEDM)* (IEEE, 2021) pp. 1–4.
 - [13] A. M. J. Zwerver, T. Krähenmann, T. F. Watson, L. Lampert, H. C. George, R. Pillarisetty, S. A. Bojarski, P. Amin, S. V. Amitonov, J. M. Boter, R. Caudillo, D. Correias-Serrano, J. P. Dehollain, G. Droulers, E. M. Henry, R. Kotlyar, M. Lodari, F. Lüthi, D. J. Michalak, B. K. Mueller, S. Neyens, J. Roberts, N. Samkharadze, G. Zheng, O. K. Zietz, G. Scappucci, M. Veldhorst, L. M. K. Vandersypen, and J. S. Clarke, *Nat Electron* **5**, 184 (2022).
 - [14] J. Ziegler, F. Luthi, M. Ramsey, F. Borjans, G. Zheng, and J. P. Zwolak, *Phys. Rev. Applied* **19**, 1 (2023).
 - [15] J. Klos, J. Tröger, J. Keutgen, M. P. Losert, N. V. Abrosimov, J. Knoch, H. Bracht, S. N. Coppersmith, M. Friesen, O. Cojocaru-Mirédin, L. R. Schreiber, and D. Bougeard, *Advanced Science* **11**, 2407442 (2024).
 - [16] S. Neyens, O. K. Zietz, T. F. Watson, F. Luthi, A. Nethewala, H. C. George, E. Henry, M. Islam, A. J. Wagner, F. Borjans, E. J. Connors, J. Corrigan, M. J. Curry, D. Keith, R. Kotlyar, L. F. Lampert, M. T. Mądzik, K. Millard, F. A. Mohiyaddin, S. Pellerano, R. Pillarisetty, M. Ramsey, R. Savytsky, S. Schaal, G. Zheng, J. Ziegler, N. C. Bishop, S. Bojarski, J. Roberts, and J. S. Clarke, *Nature* **629**, 80 (2024).
 - [17] T. Struck, A. Hollmann, F. Schauer, O. Fedorets, A. Schmidbauer, K. Sawano, H. Riemann, N. V. Abrosi-

- mov, Ł. Cywiński, D. Bougeard, and L. R. Schreiber, [npj Quantum Inf](#) **6**, 1 (2020).
- [18] D. Degli Esposti, L. E. A. Stehouwer, Ö. Gül, N. Samkharadze, C. Déprez, M. Meyer, I. N. Meijer, L. Tryputen, S. Karwal, M. Botifoll, J. Arbiol, S. V. Amitonov, L. M. K. Vandersypen, A. Sammak, M. Veldhorst, and G. Scappucci, [npj Quantum Inf](#) **10**, 32 (2024).
- [19] M. Volmer, T. Struck, A. Sala, B. Chen, M. Oberländer, T. Offermann, R. Xue, L. Visser, J.-S. Tu, S. Trellenkamp, Ł. Cywiński, H. Bluhm, and L. R. Schreiber, [npj Quantum Inf](#) **10**, 10.1038/s41534-024-00852-7 (2024).
- [20] B. Paquelet Wuetz, D. Degli Esposti, A.-M. J. Zwerver, S. V. Amitonov, M. Botifoll, J. Arbiol, L. M. K. Vandersypen, M. Russ, and G. Scappucci, [Nat Commun](#) **14**, 1385 (2023).
- [21] R. M. Wallace and G. D. Wilk, [Critical Reviews in Solid State and Materials Sciences](#) **28**, 231 (2003).
- [22] V. Brackmann, M. Neul, M. Friedrich, W. Langheinrich, M. Simon, P. Muster, S. Pregl, A. Demmler, N. Hanisch, M. Lederer, K. Zimmermann, J. Klos, F. Reichmann, Y. Yamamoto, M. Wislicenus, C. Dahl, L. R. Schreiber, H. Bluhm, and B. Lilienthal-Uhlig, in *38th European Mask and Lithography Conference (EMLC 2023)*, edited by U. F. Behringer, H. Loeschner, and J. Finders (SPIE, 2023) p. 36.
- [23] A. Elsayed, M. M. K. Shehata, C. Godfrin, S. Kubicek, S. Massar, Y. Canvel, J. Jussot, G. Simion, M. Mongillo, D. Wan, B. Govoreanu, I. P. Radu, R. Li, P. Van Dorpe, and K. De Greve, [npj Quantum Inf](#) **10**, 1 (2024).
- [24] M. Kępa, Ł. Cywiński, and J. A. Krzywda, [Appl. Phys. Lett.](#) **123**, 34003 (2023).
- [25] E. J. Connors, J. Nelson, H. Qiao, L. F. Edge, and J. M. Nichol, [Phys. Rev. B](#) **100**, 1 (2019).
- [26] C.-T. Huang, J.-Y. Li, K. S. Chou, and J. C. Sturm, [Appl. Phys. Lett.](#) **104**, 243510 (2014).
- [27] J. Ferrero, T. Koch, S. Vogel, D. Schroller, V. Adam, R. Xue, I. Seidler, L. R. Schreiber, H. Bluhm, and W. Wernsdorfer, [Appl. Phys. Lett.](#) **124**, 204002 (2024).
- [28] E. Kawakami, P. Scarlino, D. R. Ward, F. R. Braakman, D. E. Savage, M. G. Lagally, M. Friesen, S. N. Copper-smith, M. A. Eriksson, and L. M. K. Vandersypen, [Nature Nanotech](#) **9**, 666 (2014).
- [29] T. McJunkin, E. R. MacQuarrie, L. Tom, S. F. Neyens, J. P. Dodson, B. Thorgrimsson, J. Corrigan, H. E. Ercan, D. E. Savage, M. G. Lagally, R. Joynt, S. N. Coppersmith, M. Friesen, and M. A. Eriksson, [Phys. Rev. B](#) **104**, 85406 (2021).
- [30] G. Scappucci, C. Kloeffer, F. A. Zwanenburg, D. Loss, M. Myronov, J.-J. Zhang, S. De Franceschi, G. Katsaros, and M. Veldhorst, [Nat Rev Mater](#) **6**, 926 (2020).